RESEARCH ARTICLE

Macromolecular Materials and Engineering
Open Access
www.mame-journal.de

Light-Processed 3D Bioprinting of Symblepharon Rings Fortified with L-Ascorbic Acid for Ocular Tissue Engineering

Musa Ayran, Yeliz Goyuk, Aysegul Tiryaki, Songul Ulag, Ayse Ceren Calikoglu Koyuncu, Semra Akkaya Turhan, and Oguzhan Gunduz**

This study aims to develop gelatin methacryloyl (GelMA)-based symblepharon rings fortified with L-ascorbic acid (lAA), aiming for controlled release of vitamins for the treatment of the ocular surface, corneal healing, and acceleration of epithelial growth, while concurrently preventing potential inflammation. The human tears contain abundant lAA, which serves a protective role for ocular tissues. The utilization of 3D printing digital light processing technology not only navigating the manufacturing process of symblepharon rings, addressing challenges related to commercial production and expedited delivery to patients but also imparts enhanced flexibility compared to commercial products. This innovative approach also facilitates the production of rings that exhibit superior softness and are amenable to mechanical movements for ocular tissue engineering. The morphological, chemical, rheological, biological, thermal, and drug-release characteristics of 3D-printed lAA-loaded symblepharon rings are investigated. In the morphological characterization, it is observed that the rings exhibit a porous structure. In biocompatibility tests, Gelas and Gelas-low rings achieve over 75% viability. Following the cell test, scanning electron microscope images reveal fibroblasts adhering to Gelas and Gelas-low rings, spreading across their surfaces. Drug release studies conducted in phosphate-buffered saline at pH 7.4 reveal the complete release of lAA from Gelas-low within a 5-d incubation period.

1. Introduction

Symblepharon involves adhesion of the conjunctival surfaces and/or cornea in the fornix, often caused by various factors, including chemical injuries, infections, autoimmune diseases, and medications. This condition can lead to dry eyes, restricted eye movement, and an abnormal appearance.[1] Even with extensive removal of fibrovascular tissue, symblepharon has a high recurrence rate. Different methods and approaches have been developed for the successful treatment of symblepharon. Some methods developed in the 1950s aimed to prevent physical adhesion between injured conjunctival surfaces.[2] However, some of these methods have failed to keep the surfaces apart during the healing of the epithelial tissue, leading to further inflammation of the conjunctival tear. Symblepharon is a condition that is easy to diagnose but difficult to treat and there is currently no standard surgical treatment.[3] The severity of symblepharon depends on the degree of the initial injury, but early and effective treatment plays a critical role in reducing symptoms.[4]

M. Ayran, Y. Goyuk, A. Tiryaki, S. Ulag, A. C. C. Koyuncu, O. Gunduz
Center for Nanotechnology and Biomaterials Application and Research (NBUAM)
Marmara University
Istanbul 34722, Turkey
E-mail: songul.ulag@marmara.edu.tr; ucemogu@ucl.ac.uk

M. Ayran, A. Tiryaki
Department of Metallurgical and Materials Engineering, Institute of Pure and Applied Sciences
Marmara University
Istanbul 34722, Turkey

Y. Goyuk
Department of Bioengineering, Faculty of Engineering
Marmara University
Istanbul 34722, Turkey

S. Ulag
Health Institutes of Turkey (TUSEB)
Istanbul 34718, Turkey

S. Ulag, A. C. C. Koyuncu, O. Gunduz
Department of Metallurgical and Materials Engineering, Faculty of Technology
Marmara University
Istanbul 34722, Turkey

S. A. Turhan
Department of Ophthalmology
Marmara University School of Medicine
Istanbul 34854, Turkey

The ORCID identification number(s) for the author(s) of this article can be found under https://doi.org/10.1002/mame.202400057

DOI: 10.1002/mame.202400057

The ideal treatments aim to maximize corneal re-epithelialization, minimize structural abnormalities, and minimize corneal vascularization/conjunctivalization. The therapies that are to be developed should support epithelial healing, reduce inflammation, and prevent tissue loss and new wound formation. In drug therapies, L-ascorbic acid (topical and systemic), citrates, oral tetracyclines, topical corticosteroids, lubricating gels, antibiotics, therapeutic contact lenses, and tenoplasty are commonly used.[5] Amniotic membrane transplantation (AMT) is another approach that has been used in the surgical treatment of chronic symblepharon. AMT is based on the unique properties of the amniotic membrane (AM).[6,7] AM is the innermost layer of the placenta and contains various cytokines that can biologically stimulate epithelial proliferation, anti-inflammation, antiscarring, antiangiogenesis and supporting reshaping in the treatment of ocular burns.[8] The use of fibrin adhesives for AM fixation has been suggested, but their standard use has not been successful.[9] Therefore, it is very important to develop new systems that can mechanically separate the palpebral and bulbar conjunctiva without any surgical procedure, can be customized for each patient, are cost-effective, and reduce the disadvantages of surgical procedures and sutured techniques used in the treatment of symblepharon.

Symblepharon rings have been one of the most effective materials used for the prevention of symblepharon for many years, both in adults and children, without the need for a surgical procedure.[10] Symblepharon rings are transparent, hollow rings, typically made of polymethylmethacrylate material. They are placed on the eye surface to prevent the adhesion of the eyelids and conjunctiva. They are widely used in the prevention of symblepharon formation. Symblepharon ring has beneficial effects by reducing scarring and keeping the eyelids away from the damaged ocular surface.[11] Symblepharon rings also play an important role in suture less AMT techniques but it does not extend to the fornices. AM cannot cover the ocular surface because it remains beyond the cornea and perilimbal conjunctiva. However, challenges arise, such as patient discomfort linked to the rigidity of symblepharon rings and the requirement for membrane suturing in certain cases. Addressing these limitations, the development of novel ring designs is imperative to enhance patient comfort and optimize treatment efficacy.[12]

L-ascorbic acid is a powerful antioxidant that provides protective effects against many diseases, including oxidative imbalances that can occur in the cornea due to various causes.[13] Studies have shown that vitamin C can play a protective role in corneal disease repair by inhibiting the infiltration of inflammatory cells, controlling corneal neovascularization, and inflammation.[14] Gelatin methacryloyl (GelMA), a versatile biomaterial, facilitates 3D structural scaffold creation, mimicking extracellular matrix (ECM), and promoting cellular growth. With cell binding Arginine-glycine-aspartic acid (RGD) motifs and matrix metalloproteinase peptides, GelMA supports diverse cell types. Compared to amniotic membrane, GelMA reduces scarring, inflammation, and enhances epithelialization. Moreover, 3D-printed GelMA hydrogel has been shown to support epithelialization, mechanically align with tissue, and maintain a moist environment.[15–17]

Digital light processing (DLP)-based 3D printing technology is a technique that uses a projector (light source) to produce pre-designed structures and photocrosslinked materials. This technique is an ideal method for shape calibration as well as offering fast print speed and high resolution.[18] The DLP device utilized operates at a wavelength of 405 nm, thus lithium phenyl-2,4,6-trimethylbenzoylphosphinate (LAP) was employed as a photoinitiator.[19] LAP is a commonly utilized photoinitiator due to its ability to maintain high cell viability over extended periods of printing and to delay degradation by producing a low pore size.[19,20] In methacrylate-based photocurable systems, the polymerization process is initiated by the formation of radical fragments. This mechanism, driven by radicals, facilitates the production of intricate structures with superior resolution and accuracy in a wide range of photopolymerization applications[21].

In this study, the production of GelMA-based L-ascorbic acid-loaded symblepharon rings using a DLP printer will be explored for the treatment of symblepharon resulting from ocular chemical/thermal burns. The 3D printed symblepharon rings will undergo comprehensive morphological, chemical, thermal, mechanical, physical, and biological characterization. In addition, the objective is to produce symblepharon rings that are softer, more flexible, and biocompatible to prevent the disadvantages and issues associated with conventional material and methods.

2. Experimental Section

2.1. Chemical Reagents and Materials

Gelatin methacryloyl (GelMA) was produced by Type A Gelatin from porcine skin. Gelatin was acquired from Sigma Aldrich, USA. Dulbecco's phosphate buffered saline (DPBS) with a pH of 7.4 was purchased from Thermo Fisher Scientific. The LAP, with a purity exceeding 95% and a molecular weight of 294.21 g mol^{-1}, was obtained from Sigma Aldrich, USA. L-Ascorbic acid (lAA) (99+, extra pure) was obtained from Thermo Fisher Chemical.

2.2. Synthesis of Porcine Gelatin Methacryloyl (GelMA)

Porcine type A gelatin (300 bloom, Merck KGaA, Darmstadt, Germany) was chemically transformed into GelMA via methacrylation. Briefly, 300 g of gelatin was dissolved in 1 L of 0.1 M carbonate-bicarbonate buffer (CB) (pH 9) at 50 °C under magnetic stirring (500 rpm). The influence of phosphate-buffered saline (PBS) on the synthesis of GelMA was also investigated. To evaluate the buffer effect, two reaction setups were employed Methacrylic anhydride (94%) was then added dropwise, maintaining the reaction temperature at 50 °C for 3 h. To facilitate methacrylation and control the pH at 9, 5 M sodium hydroxide was employed. The reaction was quenched by adjusting the pH to 7.4 using 6 M hydrochloric acid. The resulting GelMA solution was dialyzed against ultrapure water (14 kDa cutoff) at 37 °C for 7 d to remove unreacted chemicals and salts. Finally, the dialyzed GelMA was lyophilized and stored at −20 °C for future use.

2.3. The Degree of Functionalization (DOF) Determination

GelMA and unmodified gelatin was analyzed using ^{1}H-NMR spectroscopy. A GelMA solution was prepared with a concentration of 20 mg/0.75 mL in D_2O, and ^{1}H-NMR spectra were

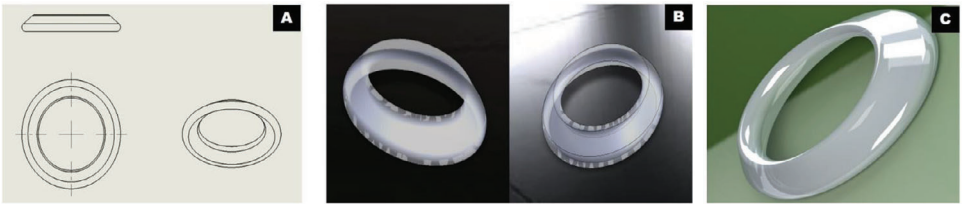

Figure 1. A) Simple design of the symblepharon ring, B) view of the inner and outer surfaces of the ring from different angles, and C) design of the 3D model.

collected at room temperature. To quantify the degree of functionalization using ^{1}H-NMR, the spectra were normalized to the phenylalanine signal (7–7.5 ppm). The integration of lysine methylene signals (2.8–2.95 ppm) from both gelatin and GelMA spectra was performed to determine the respective areas. After baseline correction, the areas of the peaks were integrated. The degree of methacrylation was calculated using Equation (1).

$$\text{DOF}\,(\%) = 1 - (\text{GelMA lysine methylene area} / \text{Gelatin lysine methylene area}) \quad (1)$$

2.4. Preparation of GelMA-Based Solutions

Three GelMA-based solutions with varying lAA concentrations (1%, 5%, and 10% v/v, referred to as Gelas-low, Gelas-medium, and Gelas-high, respectively) were prepared in 1 mL of DPBS. Each solution was magnetically stirred at 40 °C for ≈1 h to ensure complete dissolution and homogeneity. The preparation followed a specific sequence: 10% v/v GelMA was first dissolved in DPBS, followed by the addition of the respective lAA concentration. After achieving a homogeneous mixture, 5 mg mL^{-1} of LAP photoinitiator was added to render the solutions photocurable for DLP printing. As for pure 10% GelMA, it was designated as the control group for comparison with the lAA-containing rings.

2.5. The Design and 3D Printing Parameters of Symblepharon Rings

The geometry of symblepharon rings was modeled in a computer-aided design program to closely mimic the intricate contours of the eyeball and eyelid in **Figure 1**. This anatomical fidelity ensures optimal interaction and functional efficacy in cell culture. Pure GelMA and lAA-loaded solutions were subsequently utilized for 3D printing of the rings using DLP printer (Anycubic Photon D2). Customized settings were employed, including a layer thickness of 0.050 mm, exposure time of 25 s, and off time of 1 s. For optimized biocompatibility and precise printing resolution, a custom-designed, smaller resin vat with dimensions of 20 mm x 20 mm was employed. Following the printing and curing process, the rings were carefully removed from the platform using a spatula. To remove any residual printing residues, the rings were gently rinsed with deionized water. In the aftermath, they were dried using absorbent paper and subjected to freeze-drying for 2 h to ensure complete dehydration and preservation of their intricate structure.

2.6. Characterization of Symblepharon Rings

Scanning electron microscope (SEM) was performed using an EVO LS-10 system (ZEISS, Germany) to investigate the morphological characteristics of the symblepharon rings. To improve conductivity and enhance image quality, the samples were sputter-coated with gold for 60 s using a Quorum SC7620 coating system. This gold coating facilitated the precise visualization and analysis of the intricate morphological features on the ring surfaces.

Chemical characterization of the symblepharon rings was performed using Fourier-transform infrared (FT-IR) spectroscopy. To identify the functional groups, the FT-IR analysis was conducted on a Jasco 4600 FT-IR spectrometer (Japan) with a high resolution of 4 cm^{-1}, a scan rate of 32 cm^{-1}, and a wavenumber range of 4000–400 cm^{-1}.

Differential scanning calorimetry (DSC) was employed to investigate the thermal behavior of the symblepharon rings. Analyses were performed on a DSC-6O Plus instrument (Shimadzu, Japan) under a controlled nitrogen atmosphere (30–40 mL min^{-1}).[22] Weighed precise amounts of ring were hermetically sealed in aluminum pans with pierced lids to prevent pressure buildup during heating. The temperature program comprised a heating ramp from −25 to 325 °C at a constant rate of 10 °C min^{-1}.

Thermogravimetric analysis (TGA) of Gelas, Gelas-low, Gelas-medium, and Gelas-high rings was carried out with a Perkin Elmer STA 6000 from USA in order to analyze their thermal stability. Rings were heated from room temperature up to 400 °C at a constant rate of 10 °C min^{-1} under a nitrogen flow.

The mechanical properties of the symblepharon rings were evaluated using a Shimadzu EZ-LX universal testing machine (Tokyo, Japan). The force was set to 0.1 N, and the crosshead speed was maintained at 5 mm min^{-1}. Critically, the rings were prepared for testing without being cut in their own form, preserving their complete geometry, and potentially influencing the measured mechanical properties.

To examine the swelling behavior of the symblepharon rings, a gravimetric swelling test was conducted. In this study, the rings underwent immersion in PBS and were incubated at 37 °C over a 36-h period, with data collected at various time intervals. The experimentation was performed using a BIOSAN TS-100C

thermoshaker, operating at 250 rpm. This comprehensive analysis provides insights into the dynamic swelling characteristics of the symblepharon rings under controlled conditions. Using the following Equation (2), the swelling ratio of the rings was calculated.

$$\text{Swelling rate} = \frac{W_w - W_d}{W_d} \times 100 \quad (2)$$

The values of wet and dry weight were demonstrated by W_w and W_d, respectively.

Prior to the degradation test, each ring was meticulously weighed to determine its initial mass (W_o), serving as a baseline for subsequent comparisons with the final mass (W_t) following the degradation period. The degradation assay mimicked physiological conditions by incubating the rings in tubes containing 0.5 mL of PBS at 37 °C, akin to human body temperature. At specific time intervals, the spent PBS solution was carefully removed, and the open-lid tubes were returned to the oven at 37 °C for another 24 h to facilitate complete drying of the rings. This sequential wet-dry cycle mimicked the dynamic in vivo environment and ensured accurate weight measurements after each cycle. The subsequent degradation cycle involved replenishing the tubes with fresh PBS solution.[23] The degradation was calculated by using the following equation.

$$\text{Degradation rate} = \frac{W_o - W_t}{W_o} \times 100 \quad (3)$$

Rotational rheometer, utilizing the Lamy RM 200 from Lamy Rheology Instruments (Champagne au Mont d'Or, France), was employed for comprehensive rheological assessments. Equipped with the MK-PP25 measuring system and a laboratory thermostat, the rheometer conducted measurements at three distinct temperatures: 25 °C (ambient temperature), 37 °C (normal human skin temperature), and 50 °C. The inclusion of 50 °C in the analysis aimed to simulate conditions relevant to potential applications, such as those involving elevated temperatures or specific heating processes. Flow and viscosity curves were systematically generated under controlled shear conditions, ranging from 1 to 1000 s^{-1}, over a 150-s duration. The collected data, ≈40–50 data points, underwent both graphical and mathematical analyses using the Rheotex Software.

The symblepharon ring (dry) was fully hydrated in a solution prepared with PBS and subsequently cut into small pieces (1 cm x 1 cm). The prepared sample was housed in a cuvette containing 2 mL of distilled water. The optical transparency of the sample was measured in the range of 400–700 nm using a UV–vis spectrophotometer (UV-1280, Shimadzu).A PBS solution was employed as a blank for calibration purposes.[24] The optical transparency (%) was calculated using the formula:

$$\text{Optical transparency}\,(\%) = 10^{(-\text{absorbance})} \times 100 \quad (4)$$

2.7. In Vitro Drug Release Study

The in vitro release kinetics of lAA from the 10% GelMA rings were investigated in PBS, (pH 7.4) using a thermal shaker (BIOSAN TS-100C). Prior to the release study, a standard calibration curve for lAA was established using five concentrations (2.5, 5, 7.5, 10, and 12.5 μg mL^{-1}) in the 220–330 nm wavelength range on a UV–vis spectrophotometer (Shimadzu, Japan). The absorbance at 265 nm was used to quantify the lAA concentration. Subsequently, the cumulative release behavior of lAA from the rings was monitored over time. Briefly, preweighed ring segments (5 mg) were immersed in individual Eppendorf tubes containing 1 mL of fresh PBS (pH 7.4). The released lAA concentration was quantified at various time intervals by measuring the absorbance of the supernatant solution after replacing the incubation medium with fresh PBS for each subsequent measurement.

2.7.1. Drug Release Kinetic Models

To elucidate the underlying drug release mechanism, the in vitro release data were analyzed by fitting them to established kinetic models. These models included the zero-order model, the first-order model, the Higuchi model, and the Korsmeyer-Peppas model. The goodness-of-fit for each model was assessed using the correlation coefficient (R^2). Among these models, the one exhibiting the highest R^2 value was considered the most representative of the observed release kinetics. Furthermore, to gain deeper insights into the dominant release mechanism, the data were additionally analyzed using the Korsmeyer-Peppas model:

$$M_t/M_\infty = K \times t^n \quad (5)$$

M_t/M_∞ denotes the fraction of drug released at time t, K represents the rate constant, and the exponent "n" signifies the drug transport mechanism, providing a means to assess the diffusion mechanism.[25] By combining the R^2 values from the various models and the interpretation of the diffusion exponent from the Korsmeyer-Peppas model, a well-founded explanation for the drug release mechanism could be proposed.

2.8. Cell Study

In cell culture, 3-(4,5-dimethylthiazol-2-yl)-5-(3-carboxymethoxyphenyl)-2-(4-sulfophenyl)-2H-tetrazolium (MTS) assay serves as a crucial tool for the quantitative assessment of cellular viability. Prior to the MTS assay, DLP 3D-printed symblepharon rings were prepared for cell culture by sterilizing them with ethanol and penicillin. The symblepharon rings were first immersed in a 70% ethanol solution for 5 min, followed by 10 min in a 1% penicillin solution, and then rinsed thoroughly with PBS.

To assess the biocompatibility of rings, we conducted a cell viability assay using NIH-3T3 mouse embryonic fibroblasts. The rings underwent sterilization via UV exposure for 30 min before being seeded with 50 000 cells per ring. CellTiter 96 AQueous One Solution Cell Proliferation Assay (Promega) was performed on the first, 4th, and 7th days of culture, following the manufacturer's protocol.

In brief, 100 μL of culture media was combined with 20 μL of MTS for each ring. After a 2.5-h incubation period, optical density values were measured at 490 nm using a microplate

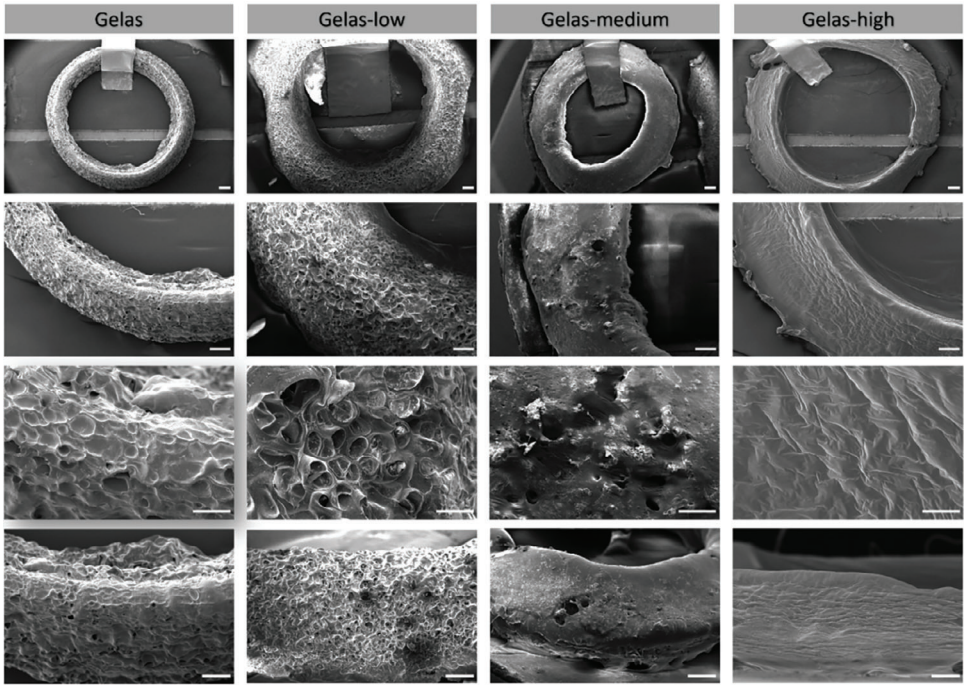

Figure 2. SEM images of Gelas, Gelas-low, Gelas-medium, and Gelas-high rings, illustrating the effect of lAA on the surface morphology of the rings. The first row shows the front view of the rings at 20x magnification. The second and third rows show regional images of the rings at 50x and 100x magnification, respectively. The fourth row depicts the side view of the rings at 50x magnification.

spectrophotometer (Agilent BioTek, Epoch2). Optical density (OD) 490 values were then converted to cell numbers utilizing a calibration curve tailored for 3T3 cells.

Mouse fibroblast-laden rings were examined by SEM at days 1 and 3 of culture to assess their morphology. Following culture media removal, the rings were rinsed with 0.1 M cacodylate buffer (pH 7.4) and fixed in 2.5% glutaraldehyde for 20 min. To prepare for SEM analysis, the specimens were then freeze-dried for 2 h.

3. Results and Discussion

The functional significance of pore structures in porous polymers for tissue engineering lies in their ability to control cell functions and guide the formation of new tissues and organs. These pores act as conduits for cell seeding, enabling penetration and distribution throughout the surface of structures, ultimately directing the development of desired tissue architectures.[26] Given the crucial role of the cellular microenvironment in tissue regeneration, SEM was used to obtain morphological images of symblepharon rings in **Figure 2**. These images reveal that Gelas displays porous structures across its surface. Even with the addition of lAA at low concentrations, Gelas-low retains similar porous structures. In Gelas-medium, porous structures appeared in certain regions on the surface where most of the porous structures were closed. In Gelas-high, all pores were closed, resulting in a poreless structure. Additionally, it was found that the printing quality of Gelas-medium and Gelas-high structures decreased, with breaks and deformations occurring.

The extent of methacrylation in GelMA was assessed through ^{1}H-NMR spectrometry. The acquired ^{1}H-NMR spectra for GelMA synthesized with both PBS and CB are depicted in **Figure 3A–D** for analysis. The ^{1}H-NMR spectrum of GelMA exhibited two distinct signals at chemical shifts of 5.4 and 5.6 ppm, which are characteristic of the acrylic protons (2H) associated with the methacryloyl groups grafted onto the gelatin backbone during the synthesis of GelMA. Additional evidence for successful methacrylation comes from the presence of new peaks at 1.9 ppm for methyl protons of methacryloyl groups in the GelMA spectrum.[27] These newly observed signals provide direct evidence of the successful modification of the gelatin structure with methacrylic functionalities, enabling the formation of photopolymerizable GelMA hydrogels. Moreover, the absence of the characteristic signal at 2.91 ppm in Figure 3D, previously assigned to lysine methylene protons in unmodified gelatin, observed in the ^{1}H NMR spectrum of GelMA, strongly indicates nearly complete substitution of lysine amino groups by methacrylamide groups.[28,29] These signals can be attributed to the acrylic protons and methyl groups of the introduced methacrylamide groups, further bolstering the conclusion of extensive lysine modification. This study demonstrates the critical role of buffer selection in optimizing the DOF of GelMA. GelMA synthesized using PBS (pH 7.4) as a buffer exhibited a DOF of 78%, whereas the utilization of CB buffer resulted in a substantial increase to 87%. This disparity can be ascribed to the pH-altering effect of methacrylic acid, a side product of the reaction, which renders the PBS solution acidic. Previous studies have also shown that CB buffer can lead to higher DOF compared to PBS due to its superior pH maintenance capabilities.[30] In addition, GelMA was produced by attaching methacrylate groups to the surface of gelatin, using a chemical bond formed between the methacrylate groups and the protein's amine groups. Figure 3E illustrates this process.

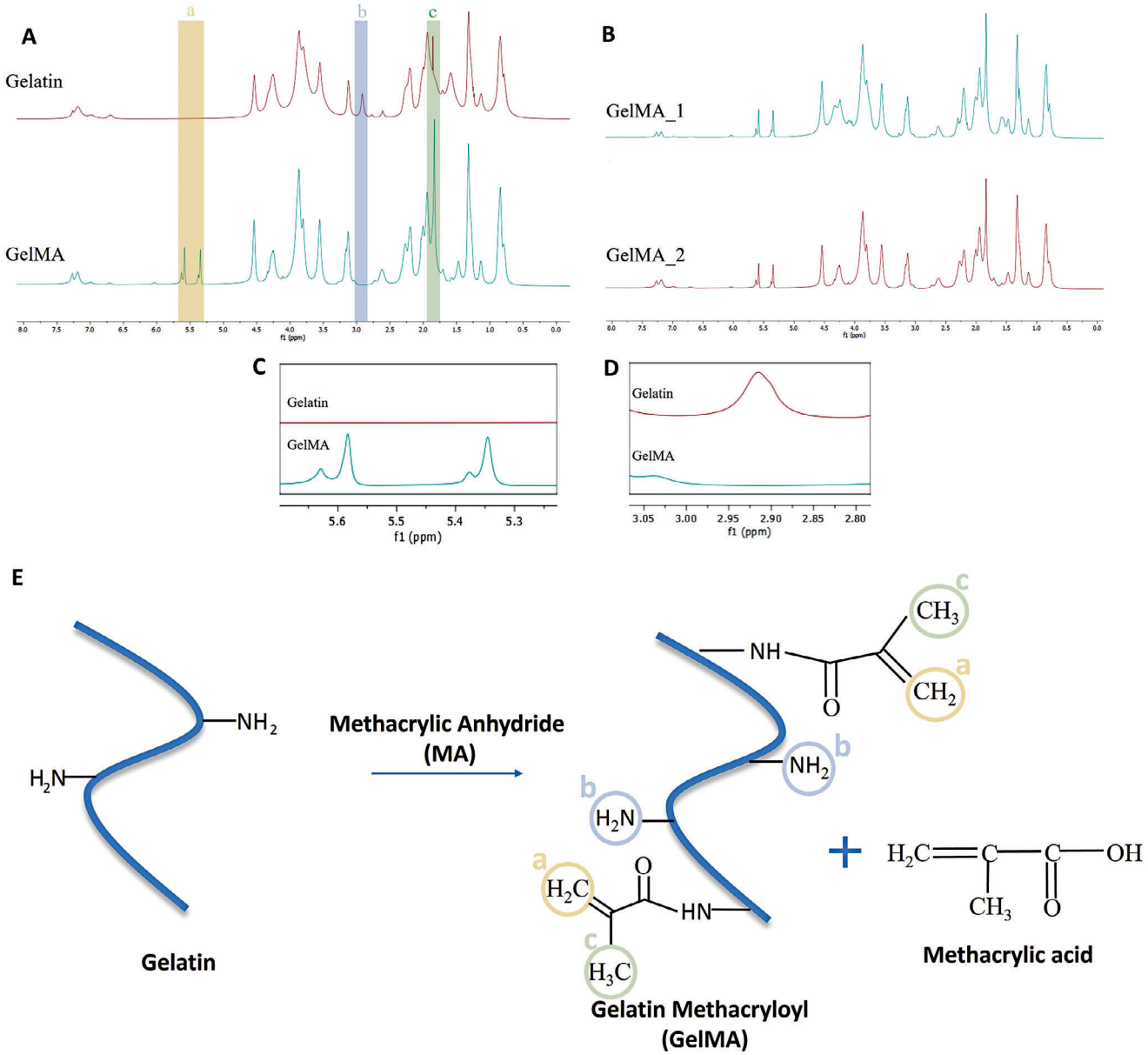

Figure 3. A) ^{1}H NMR spectra of gelatin and GelMA, peaks correspond to acrylic protons (2H) of methacrylamide groups in a) lysine and hydroxyl lysine groups, b) methylene protons (2H) of unreacted lysine groups, and c) methyl protons (3H) of methacrylamide groups. B) PBS treated GelMA_1 and CB treated gelMA_2. C) Methacryl peaks between GelMA and gelatin at ≈5.2–≈5.7 ppm, respectively, which coincide with the acrylate protons (CH2═CH(CH3)) of hydroxylysine and lysine. D) The demonstration of lysine methylene peaks of unmodified gelatin and GelMA at ≈2.91 ppm. E) Diagram depicting GelMA synthesis in correlation with ^{1}H NMR peaks.

The creation of symblepharon rings for a corneal substitute in tissue engineering necessitates the design of structures that fulfil the specific biological requirements of the cornea. The cornea's optimal mechanical properties not only provide essential structural support, elasticity, and protection for the eye, but also critically govern the biomechanical cues that guide stromal cell behavior and maintain healthy tissue function.[31] Characterization of the mechanical properties of symblepharon rings was undertaken, considering their paramount significance in optimizing the design of effective eye substitutes. **Table 1** shows the compressive strength-strain values of Gelas rings, with all rings exceeding 0.5 MPa in compressive strength. Gelas rings exhibited the highest compressive strength, reaching 1.42 ± 0.12 MPa. Gelas-low followed with a compressive strength of 1.35 MPa. Other groups demonstrated significantly lower values. This suggests a potential correlation between increasing lAA concentration and weakening of the structures, alongside a decrease in photocrosslinking capacity.

The interactions between GelMA and lAA-loaded Gelas rings were investigated using FT-IR spectroscopy (**Figure 4A**). This analysis aimed to identify potential changes in the chemical composition and functional groups of GelMA upon lAA

Table 1. The mechanical strength values of the symblepharon rings.

Symblepharon rings	Compressive strength [MPa]	Strain at break [%]
Gelas	1.42 ± 0.12	19.20 ± 2.25
Gelas-low	1.35 ± 0.17	17.40 ± 2.85
Gelas-medium	0.83 ± 0.05	21.15 ± 3.24
Gelas-high	0.60 ± 0.02	27.22 ± 3.13

incorporation. The C═C ring stretching vibrations in lAA were responsible for the absorption band at 1654 cm^{-1}, which remains unaffected in all concentrations (Gelas-high, Gelas-medium, Gelas-low). However, incorporating lAA into the rings alters the vibrational peaks, particularly in Gelas-high and Gelas-medium. Particularly, the strong band at 1752 cm^{-1} in Gelas-high is assigned to the C═O stretching mode of the five-membered lactone ring. Moreover, the C—O stretching modes contribute to the strong IR bands observed at 1024 cm^{-1}.[32] lAA also exhibited additional peaks at 3523, 3407, and 3311 cm^{-1}, attributed to the stretching vibrations of different hydroxyl groups within the molecule.[33] The Gelas ring structures exhibit characteristic peaks at 2929 cm^{-1} (C—H stretching), 1629 cm^{-1} (C═O stretching), and 1544 cm^{-1} (N—H bending coupled to C—H stretching), distinct from the peaks associated with lAA.[28] Figure 4C reveals the relationship between GelMA and gelatin powder using FT-IR spectroscopy. Precisely, a peak at 937 cm^{-1} appears in the GelMA spectrum, attributable to the C═C double bonds introduced by methacrylation.[34] Although the typical C═C stretching absorption peak at 1620–1680 cm^{-1} is typically associated with the methacrylate vinyl group, it is masked by the strong amide I signal in the GelMA spectra.[28] In GelMA, the spectral region between 3200 and 3400 cm^{-1} corresponds to the presence of the peptide bond (N—H stretching), characteristic of amide A.[35] This peak is apparently more prominent compared to Gelatin.

The degradation and swelling profiles of Gelas rings incubated at 37 °C in PBS are presented in Figure 4B,D. Compared to other

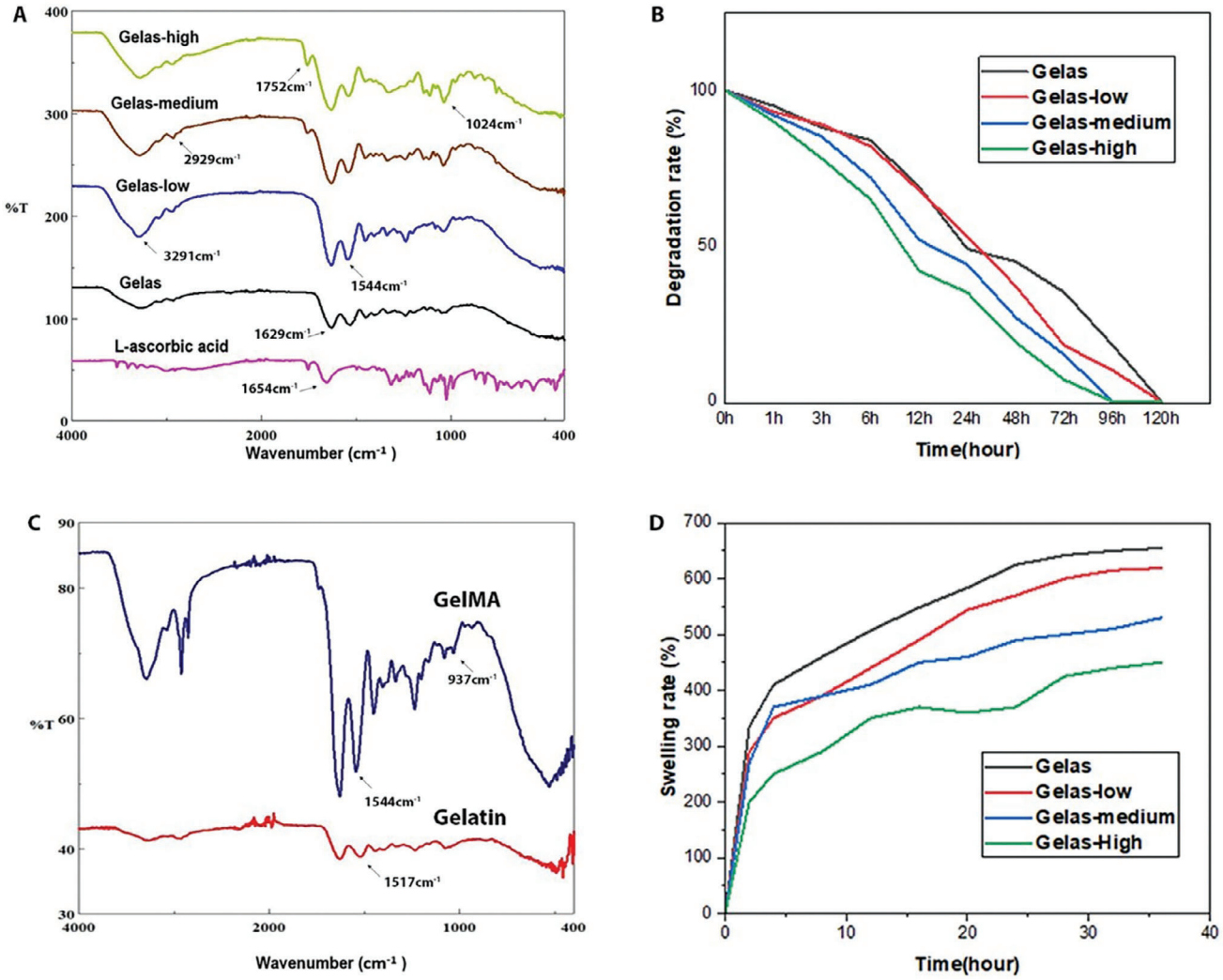

Figure 4. A) FT-IR spectra of symblepharon rings and lAA. B) Evaluation of swelling rate. C) FT-IR spectra of GelMA and gelatin powder. D) Evaluation Degradation Rate in symblepharon rings.

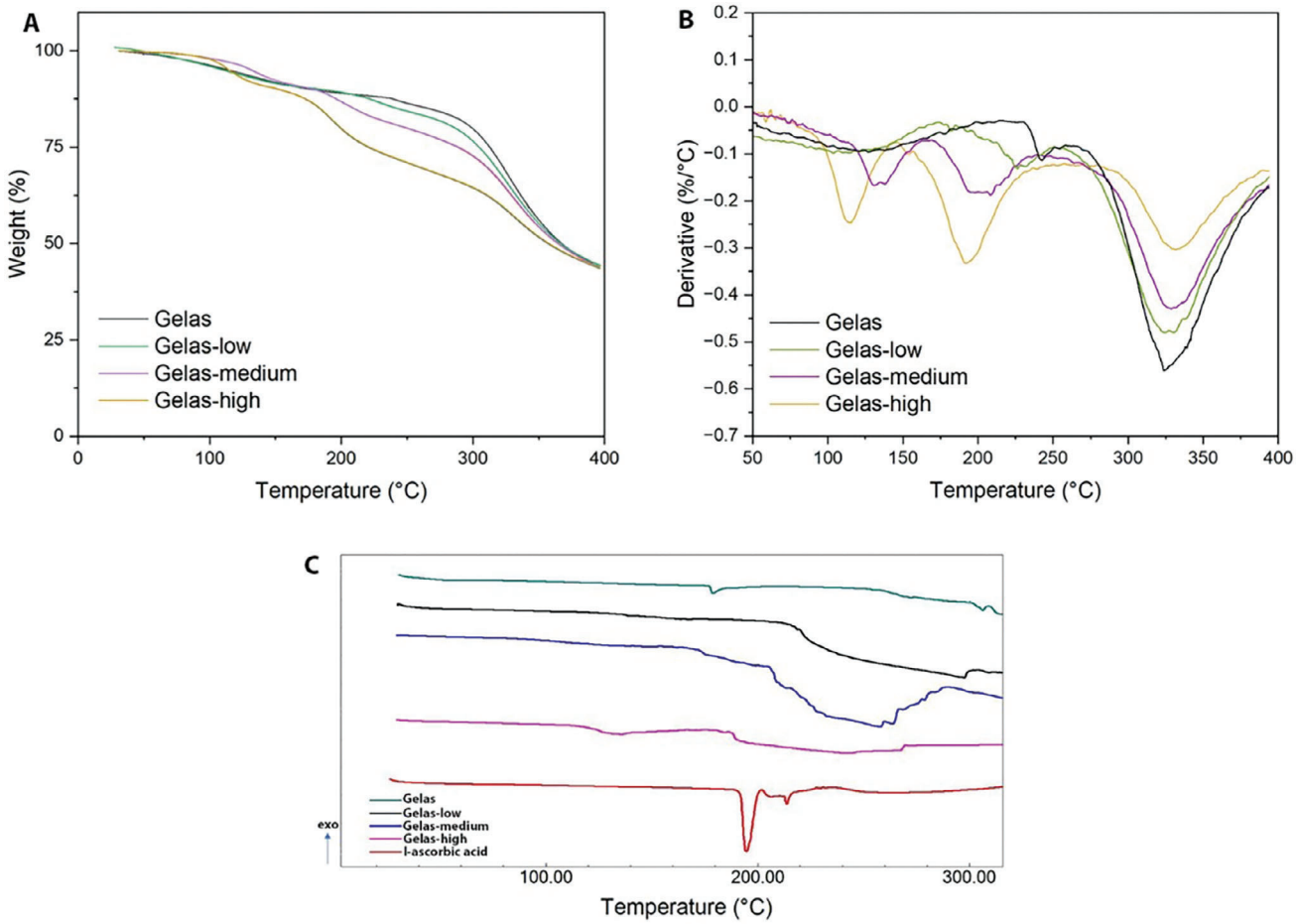

Figure 5. Thermal Analysis: A) TGA, B) DTG, and C) DSC profiles illustrating alterations in the thermal characteristics of symblepharon rings.

lAA-incorporated rings, Gelas exhibited a significantly higher swelling rate and longer degradation time. Interestingly, within 24 h of incubation, Gelas reached a swelling ratio of ≈625%, while Gelas-low, Gelas-medium, and Gelas-high displayed lower values of 570%, 490%, and 370%, respectively. As the concentration of lAA increases, a significant decrease in the swelling characteristics of the rings has been observed. Meanwhile, it has been noted that rings with higher lAA concentrations undergo faster degradation, with the Gelas-medium and Gelas-high rings completely disintegrating before the end of the 4-d observation period. In contrast, Gelas-low and Gelas rings, having experienced a relatively steady progression over the initial 4 d, exhibit complete degradation by the 5th day. These phenomena can arise from the interplay between crosslinking and the polymer network with the addition of lAA. SEM images confirmed that higher IAA concentrations closed the pores in the Gelas structures, implying insufficient crosslinking and diminished swelling capacity of the rings. This inadequate crosslinking likely contributed to the distorted ring shapes and accelerated degradation observed at higher IAA concentrations. The swelling behavior and degradation rates of a material can be manipulated through photocrosslinking, as confirmed by the scientific literature.[36] In medical studies, it is imperative for symblepharon rings to withstand degradation on the ocular surface without dissolution and to exhibit stretching against mechanical stress, ensuring their integrity throughout treatment within the damaged area. By increasing the concentration of these GelMA-derived rings, the dissolution time can be improved, as well as flexibility can be achieved by using a plasticizing biomaterial or by reducing the curing time.

Figure 5A,B depicts thermogravimetric behaviors of symblepharon rings through both TGA and derivative thermogravimetry (DTG) curves. The initial weight loss of IAA-loaded Gelas rings occurs earlier and increases rapidly compared to that of Gelas ring. While the thermal characteristic structures of Gelas and Gelas-Low exhibit similarities, those of Gelas-Medium and Gelas-High show greater resemblance to each other. This observation is attributed to the distinct weight loss patterns: Gelas and Gelas-Low exhibit a two-stage, whereas Gelas-Medium and Gelas-High display a three-stage in terms of weight loss. A first weight loss of about 4.2%,4.5%, 2.1% and 1.8% until 100 °C for Gelas, Gelas-low, Gelas-medium and Gelas-high, respectively, it may be attributed due to the presence of moisture.[37] After reaching 120 degrees, Gelas-High begins to lose weight at a faster rate compared to the other groups. This could be due to weaker crosslinking, possibly caused by the higher ratio of IAA present in this ring. In Gelas-Medium and Gelas-High, decomposition likely initiates between 185 and 210 °C owing to the higher concentration of ascorbic acid. This inference aligns with literature,

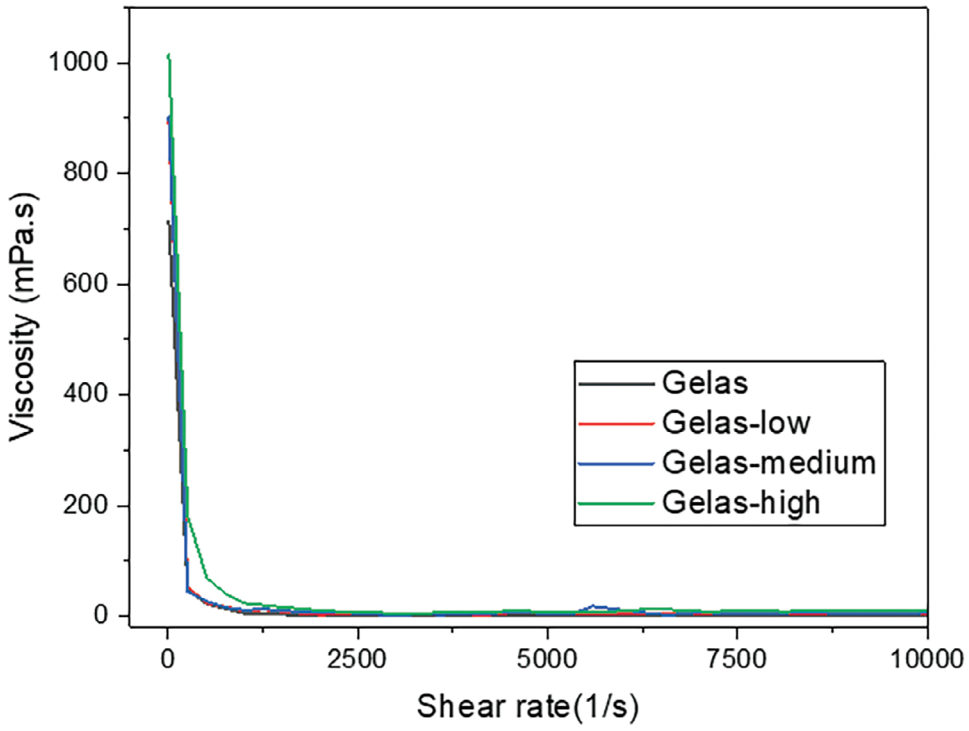

Figure 6. Shear stress–viscosity graph illustrating the rheological behavior of Gelas solutions.

which indicates a decomposition onset at 191 degrees in the thermogravimetric analysis of lAA.[38] Additionally, GelMA-induced decomposition is anticipated to commence between 300–310 °C. The maximum decomposition temperature observed at ≈324 °C across all groups may be linked to protein degradation,[39] while a weight loss of up to 50% for all groups appeared at ≈357–368 °C. Furthermore, the decomposition of Gelas was slow, and the nonvolatile residue remained was high (≈79.7 wt%) up to 300 °C.

DSC analysis revealed distinct thermal profiles for Gelas rings and lAA in Figure 5C. The thermogram of pure lAA exhibited a single endothermic peak at 195 °C, corresponding to its melting point. This melting point was absent in the DSC curves of all Gelas rings, suggesting the successful incorporation of lAA into the gels. However, the endothermic peak for composite hydrogels containing higher lAA concentrations (Gelas-medium and Gelas-high) shifted to a higher temperature compared to Gelas-low. Additionally, Gelas-high displayed a flatter baseline compared to other rings, possibly influenced by the presence of lAA. Interestingly, Gelas and Gelas-low exhibited an additional endothermic peak between 300 and 310 °C. In the TGA analysis, we also observed a similar behavior for these groups within this temperature range, which may indicate protein degradation.

It was observed a clear connection between higher shear rates and lower viscosity across all solutions in **Figure 6**, suggesting their tendency to undergo shear thinning. This behavior is likely due to the disentanglement of the polymer network in the hydrogel induced by shear. When the rate of disentanglement surpassed the rate at which the network could rebuild itself, the hydrogels thinned and flowed more easily with reduced resistance.

In **Table 2**, it was presented the viscosity-temperature values for all solutions at 25, 37, and 50 °C. A distinctive trend emerges, revealing a consistent decline in viscosity as the temperature increases across all solutions. For instance, Gelas, starting with an initial viscosity of 270 mPa s at 25 °C, experienced a decrease to 233 mPa s at 50 °C. Even Gelas-high, the solution with the highest lAA content, displayed a significant reduction, transitioning from 491 mPa s at low temperature to 302 mPa s at high temperature. This observed thinning is likely attributed to the acceleration of macromolecular motion induced by temperature. The heightened mobility disrupts the formation of weak bonds between macromolecules.[40] Moreover, the incorporation of lAA resulted in an augmentation of the viscosity in the solutions. This phenomenon can be attributed to the elevation of total solid content within the solution and the subsequent densification of the network structure, consequently contributing to an increased viscosity. Higher drug content within the 3D-printed rings appears to negatively impact printing quality, considering the Gelas-medium and Gelas-high rings. This could be attributed to an increase in rheological properties, potentially leading to greater resistance to the curing process. The rings with higher viscosity

Table 2. Viscosity profiles of Gelas ring solutions at various temperatures.

Solutions	Viscosity (mPa s) at different temperatures		
	25 °C	37 °C	50 °C
Gelas	270.66	263.64	233.28
Gelas-low	281.94	263.81	228.65
Gelas-medium	360.24	330.96	286.25
Gelas-high	491.63	349.81	302.45

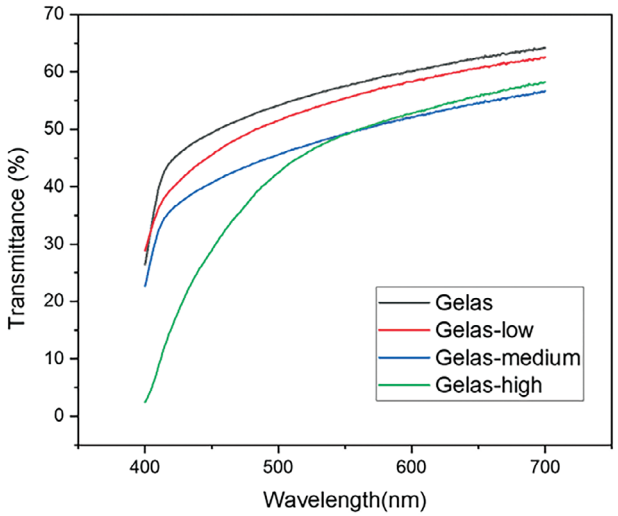

Figure 7. Optical transmittance of hydrogels.

may absorb less UV light and therefore exhibit incomplete curing compared to the lower viscosity rings.

Figure 7 illustrates the light transmittance of Gelas and lAA-loaded Gelas hydrogels as a percentage. This graphical representation highlights that hydrogels in the Gelas group exhibit the highest light transmittance, particularly demonstrating ≈66% transmittance in the range of 650–700 nm. Observations indicate that an increase in drug concentration diminishes the light-transmitting capacity of the hydrogels. When examined with respect to wavelength, an increase in transmittance around 700 nm is observed. The wavelength employed for crosslinking with UV in the DLP printer is 405 nm. However, the transmittance for this wavelength in hydrogels is observed to be in the range of 20–30%. Interestingly, in the Gelas-high group, the transmittance in this region is ≈5% due to the high concentration of drug, indicating a considerably low level. These findings contribute to our understanding of the effects of hydrogel properties and components on light transmittance at relevant wavelengths. Particularly in crosslinking processes and material optimization, these results hold significance, as light transmittance can play a critical role in hydrogel performance. The transmittance, varying with wavelength, has been observed to increase from 50% to 67% within the examined range (600–700 nm). In this context, the transmittance trend of Gelas and Gelas-low rings exhibits a structure reminiscent of the cornea in middle-aged human eyes.[41]

A modified dissolving technique in PBS at pH 7.4 was applied to investigate the in vitro release of lAA from all symblepharon rings, with the outcomes depicted in **Figure 8**. Figure 8A portrays the cumulative release profile of lAA from the symblepharon rings, while Figure 8B exhibits the absorbance graph derived from the calibration curve at 265 nm. Figure 8C showcases the calibration curve established with five concentrations (2.5, 5, 7.5, 10, and 12.5 μg mL^{-1}). The investigation demonstrated that the rings displayed similar release profiles but varied in the quantity of released lAA, depending on the incorporated lAA concentration. As depicted in the graph, the initial 30 min witnessed a release percentage of 11.56% for Gelas-high. Subsequently, after one day, ≈62.32% of lAA was primarily released from the Gelas-high ring. The accelerated release in Gelas-high is attributed to the elevated lAA concentration on the ring's surface. A discernible pattern in the release kinetics of lAA from the rings indicated a direct association between its release capacity and escalating lAA concentrations. Gelas-low exhibited a controlled and sustained drug release pattern characterized by an initial burst of 10.33% within the first hour, followed by a slower and prolonged release reaching 22.80% by 12 h and 33.48% by the end of the first day. This controlled release likely stems from the unique properties of Gelas-low, which facilitated sustained drug retention compared to other groups. Based on SEM images, Gelas-low displays a porous structure compared to Gelas-Medium and Gelas-High. The inherent interconnected channel-pore design of 3D-printed structures promotes uniform dispersion of release media, facilitating controlled drug release.[42] Additionally, the ability to adjust pore sizes, porosity levels, and surface areas offers opportunities for tailoring drug release patterns and durations to specific requirements. Remarkably, all rings achieved complete degradation within 5 d, ensuring complete drug delivery into the PBS environment. The Gelas-low ring, when strategically positioned in the chemically damaged region between the eyeball and eyelid, emerges as a potential candidate for topically delivering lAA to the damaged area in a controlled manner. Such an application could expedite the healing process within the damaged zone, presenting a promising avenue for therapeutic intervention.

Mathematical modeling is a cornerstone in the thorough investigation of drug release kinetics, providing invaluable insights into the underlying mechanisms, optimizing formulation design, and predicting in vivo performance. This powerful tool propels our understanding and refinement of drug delivery processes, ultimately enhancing their efficacy.[43] To gain insights into the release dynamics of lAA from the rings, four different mathematical models were utilized. **Figure 9**A–D illustrates the release kinetics of rings using zero-order, first-order, Higuchi, and Korsmeyer-Peppas approaches.

The corresponding kinetic constants and regression coefficients (R^2) for all lAA-loaded rings are detailed in **Table 3**. Evaluation of the most fitting mathematical model for lAA-loaded rings, based on the highest correlation coefficient, reveals that Gelas-high adheres to the first-order model of drug release. Conversely, Gelas-low exhibits compatibility with the zero-order (97.2%), Higuchi (96.9%), and Korsmeyer-Peppas (96.7%) models. Furthermore, the "*n*" values corresponding to distinct transport mechanisms were elucidated following the Korsmeyer-Peppas model. The ranges of "*n*" values shed light on the drug release mechanisms from polymeric materials.[44] As outlined in Table 3, the "*n*" value associated with the Korsmeyer-Peppas model signifies that only Gelas-low demonstrates non-Fickian transport. Consequently, the porosity of Gelas-low emerges as a significant determinant in shaping the drug transport mechanism.

The study assessed the viability, attachment, and proliferation of 3T3 fibroblast cells on symblepharon rings. As depicted in **Figure 10**, both MTS and SEM tests revealed a high cell viability for Gelas and Gelas-low. The cells displayed a fibroblast-like morphology, indicating that the rings did not induce toxicity. Figure 10A illustrates cell viabilities, with Gelas exhibiting 73% and Gelas-low showing 76% viability on the first day. After 3 d, Gelas and Gelas-low displayed viabilities of 63.5% and 68%, respectively. By day 7, Gelas and Gelas-low exhibited viabilities

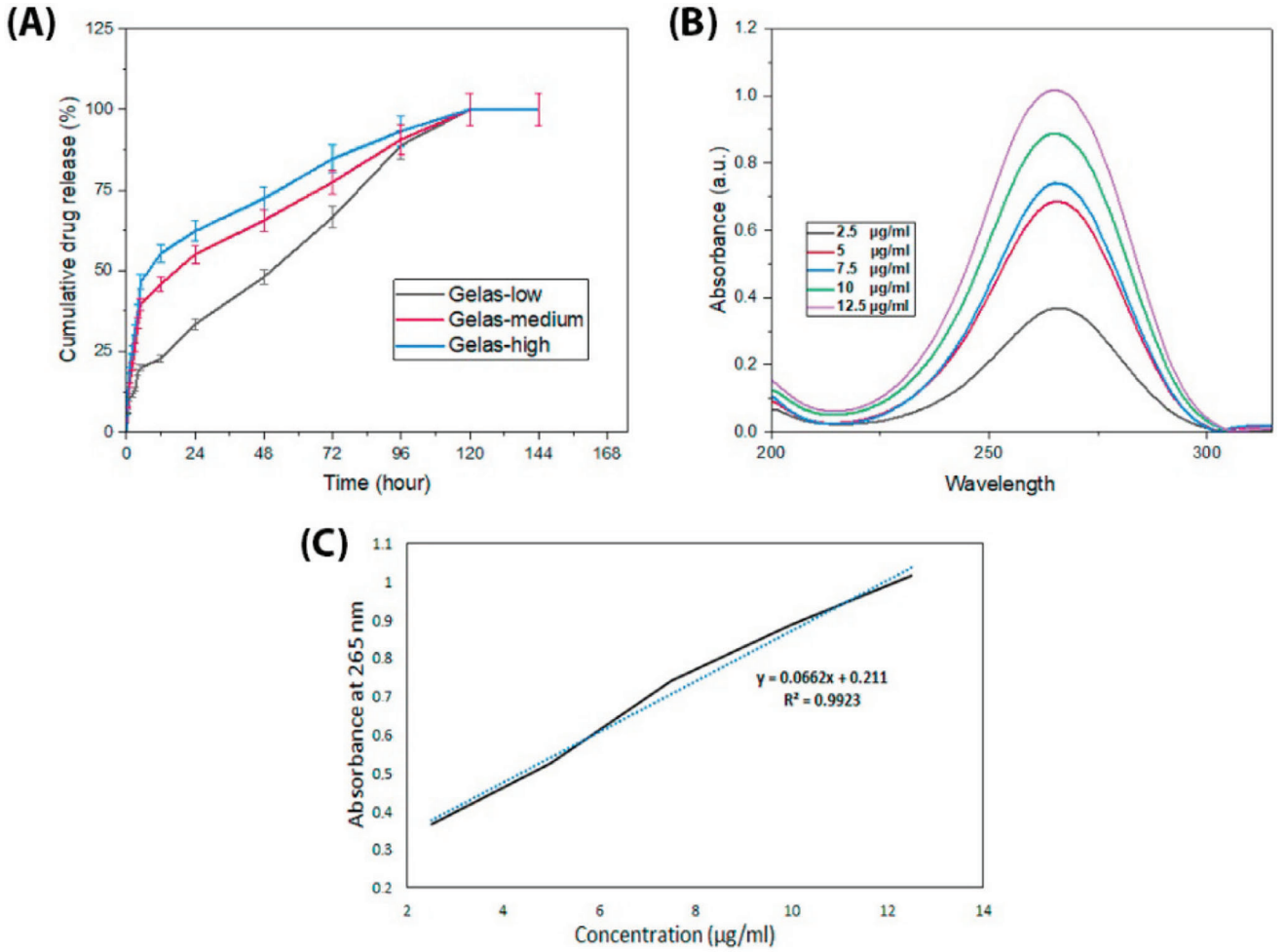

Figure 8. A) Cumulative release profiles of the IAA from the rings, B) the linear calibration curves of the IAA, and C) the absorbance graphs of the IAA at 265 nm obtained from calibration curves.

of 79% and 77%, respectively. Particularly, Gelas-high demonstrated toxic characteristics, remaining below 50%, indicating weak cell adhesion and low proliferation in these rings. The observed toxicity is attributed to the high IAA concentration and rapid degradation. In Gelas-high and Gelas-medium, both with elevated acid concentrations, the release of IAA into the medium was observed to acidify and yellow the medium. Due to the rapid dissolution of the drug in water, the pH of the medium dropped to ≈6 upon release from the ring section.[45] High IAA concentration was found to be detrimental to cell viability, leading to increased cell death. In contrast, Gelas-low did not yellow the medium and was found to support cell viability. After 7 d, Gelas-medium and Gelas-high rings were completely dissolved, while Gelas and Gelas-low rings were mostly degraded. Figure 10B depicts the cell counts of the rings over the course of 7 d, reflecting the same trend observed in cell viability. Particularly, the cell counts in the Gelas and Gelas-low groups were ≈60 000 and 55 000, respectively, after 7 d. The SEM images of fibroblast cells on Gelas and Gelas-low at 1 and 3 d are shown in Figure 10C. Examination of the SEM images revealed that the cells spread on the ring surface within 3 d, supporting cell adhesion.

Table 3. Drug release kinetics according to the ranges of n value and regression coefficients (R^2).

Symblepharon rings	Korsmeyer-Peppas		Zero-order		First-order		Higuchi	
	R^2	n	R^2	K_o	R^2	K_1	R^2	K_h
Gelas-low	0.967	0.46	0.972	0.816	0.924	−0.0081	0.969	8.132
Gelas-medium	0.956	0.36	0.825	0.795	0.952	−0.0091	0.950	8.509
Gelas-high	0.958	0.32	0.775	0.799	0.957	−0.0105	0.925	8.714

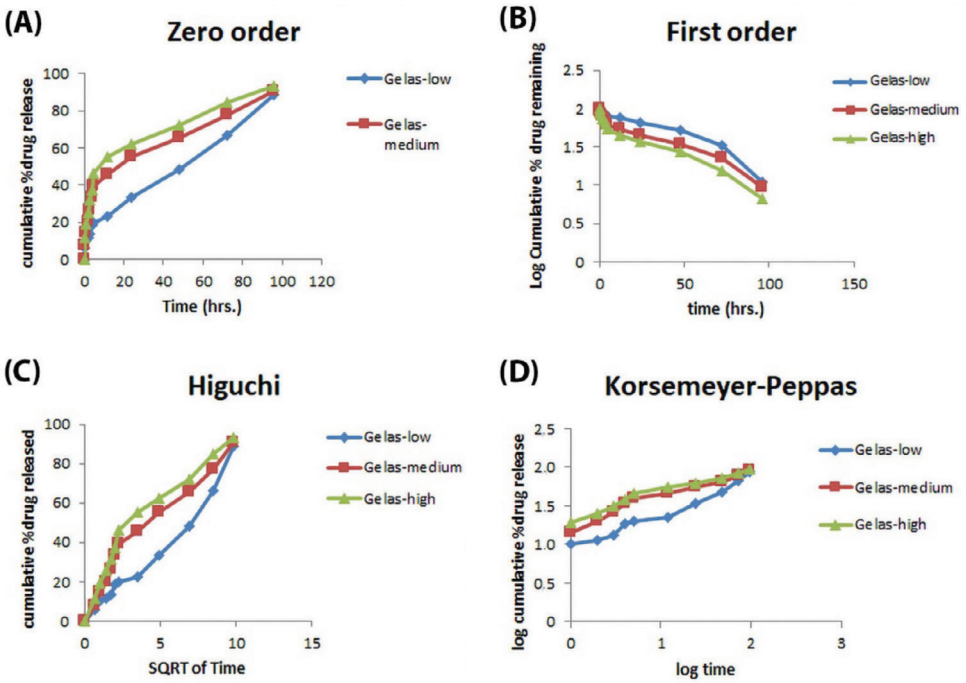

Figure 9. Comprehensive characterization of drug release kinetics including A) zero-order, B) first-order, C) Higuchi, and D) Korsmeyer-Peppas models.

4. Conclusions

In conclusion, this study successfully fabricated symblepharon rings designed for the treatment of symblepharon defects. These rings, enhanced with lAA for chemically damaged eye regions, demonstrated controlled drug release capabilities as assessed through rigorous drug release tests. The varying concentrations of IAA have been found to impact both drug release profiles and the structural integrity of GelMA-based ocular implants. High concentrations of IAA were associated with diminished structural integrity, reduced curing during 3D printing, mechanical weakness, and inadequate control over drug release. Conversely, Gelas-Low demonstrated similarities to the Gelas group across multiple parameters, suggesting that formulations closely resembling this concentration may hold promise for future clinical studies. Gelas-low also emerged as the most promising candidate based on its optimal morphology, superior drug retention capacity, and reduced toxicity. Furthermore, these rings

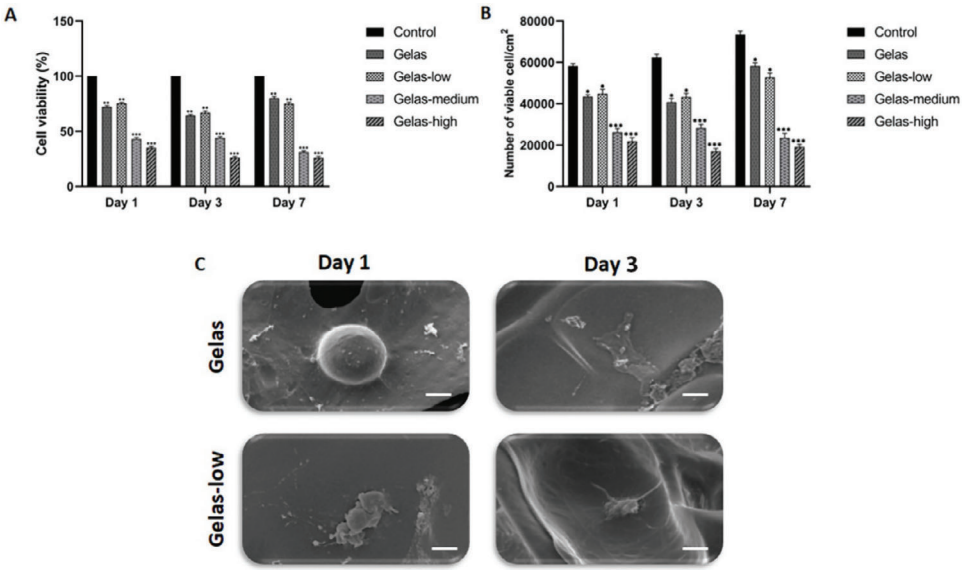

Figure 10. A) Cell viability of symblepharon rings, B) quantification of cell numbers in symblepharon rings, and C) SEM images of cell-laden Gelas and Gelas-low rings.

accomplish the essential criteria for ocular tissue engineering, offering the requisite softness and flexibility through the incorporation of organic materials. In addition, the porous structure of Gelas-low adds a critical dimension to its suitability for ocular tissue, enhancing its efficacy in drug delivery and promoting a favorable healing environment.

Acknowledgements

This study was supported financially by TUBITAK with the 222S265 project number.

Conflict of Interest

The authors declare no conflict of interest.

Data Availability Statement

The data that support the findings of this study are available from the corresponding author upon reasonable request.

Keywords

DLP printing, GelMA, L-ascorbic acid, symblepharon rings

Received: February 13, 2024
Revised: May 7, 2024
Published online:

[1] A. Venugopal, M. Ravindran, *Indian J. Ophthalmol.* **2021**, *1*, 106.
[2] A. Swarup, C. N. Ta, A. Y. Wu, *Surv. Ophthalmol.* **2022**, *67*, 19.
[3] H. Martinez-Osorio, S. A. Schellini, L. S. Marin-Muñoz, *Am. J. Ophthalmol. Case Rep.* **2021**, *23*, 101099.
[4] J. Chen, M. W. Wang, J. J. Xu, X. Y. Wu, J. Yao, *Riv. Eur. Sci. Med. Farmacol.* **2020**, *24*, 10134.
[5] M. Eslani, A. Baradaran-Rafii, A. Y. Cheung, K. H. Kurji, H. Hasani, A. R. Djalilian, E. J. Holland, *Am. J. Ophthalmol.* **2019**, *199*, 209.
[6] D. P. Parmar, P. K. Bhole, P. N. Patel, J. N. Jadeja, *Indian J. Ophthalmol.* **2021**, *69*, 58.
[7] S. Jain, A. Rastogi, *Eye (London, U. K.)* **2004**, *18*, 1251.
[8] X. Liang, Z. Liu, Y. Lin, N. Li, M. Huang, Z. Wang, *J. Burn Care Res.* **2012**, *33*, e32.
[9] T. Röck, M. Bramkamp, K. U. Bartz-Schmidt, D. Röck, *Med. Sci. Monit.* **2019**, *25*, 7976.
[10] D. G. Gregory, *Ocul. Surf.* **2008**, *6*, 87.
[11] N. Kara, *Can. J. Ophthalmol.* **2018**, *53*, e46.
[12] S. G. Honavar, A. K. Bansal, V. S. Sangwan, G. N. Rao, *Ophthalmology* **2000**, *107*, 975.
[13] G. S. Gujral, S. N. Askari, S. Ahmad, S. M. Zakir, K. Saluja, *Indian J. Ophthalmol.* **2020**, *68*, 2935.
[14] M. Li, Z. Chen, L. Liu, X. Ma, J. Zou, *J. Ophthalmol.* **2021**, *2021*, 2406646.
[15] S. Dehghani, M. Rasoulianboroujeni, H. Ghasemi, S. H. Keshel, Z. Nozarian, M. N. Hashemian, M. Zarei-Ghanavati, G. Latifi, R. Ghaffari, Z. Cui, H. Ye, L. Tayebi, *Biomaterials* **2018**, *174*, 95.
[16] E. Pilavci, M. Ayran, D. Ulubay, E. Kaya, G. Tinaz, O. Bingol Ozakpinar, A. Sancakli, O. Gunduz, *J. Bioact. Compat. Polym.* **2022**, *38*, 3.
[17] M. S. Izgordu, M. Ayran, S. Ulag, R. Yildirim, B. Bulut, A. Sahin, M. M. Guncu, B. Aksu, O. Gunduz, *Macromol. Mater. Eng.* **2023**, *308*, 2300151.
[18] M. Ayran, S. Ulag, S. Ervan, O. Gunduz, *Mater. Lett.* **2024**, *363*, 136316.
[19] K. H. Yang, G. Lindberg, B. Soliman, K. Lim, T. Woodfield, R. J. Narayan, *Polymers (Basel)* **2021**, *13*, 1877.
[20] H. Xu, J. Casillas, S. Krishnamoorthy, C. Xu, *Biomed. Mater.* **2020**, *15*, 055021.
[21] A. Bagheri, J. Jin, *ACS Appl. Polym. Mater.* **2019**, *1*, 593.
[22] A.-M. Croitoru, M. Ayran, E. Altan, Y. Karacelebi, S. Ulag, A. Sahin, M. M. Guncu, B. Aksu, O. Gunduz, B.-M. Tihăuan, D. Ficai, A. Ficai, *Int. J. Biol. Macromol.* **2023**, *253*, 126996.
[23] A. C. Puigmal, M. Ayran, S. Ulag, E. Altan, M. M. Guncu, B. Aksu, B. K. Durukan, H. T. Sasmazel, R. A. Perez, E. Koc, D. O'Callaghan, O. Gunduz, *J. Mech. Behav. Biomed. Mater.* **2023**, *148*, 106163.
[24] I. A. Barroso, K. Man, T. E. Robinson, S. C. Cox, A. K. Ghag, *Bioengineering* **2022**, *9*, 53.
[25] J. Xu, B. Xu, D. Shou, X. Xia, Y. Hu, *Polymers (Basel)* **2015**, *7*, 1850.
[26] G. Chen, N. Kawazoe, *Biomaterials Nanoarchitectonics*, **2016**, pp. 77–95.
[27] M. Zhu, Y. Wang, G. Ferracci, J. Zheng, N. J. Cho, B. H. Lee, *Sci. Rep.* **2019**, *9*, 6863.
[28] C. Li, C. Mu, W. Lin, *RSC Adv.* **2016**, *6*, 43663.
[29] H. Yin, M. Zhu, Y. Wang, L. Luo, Q. Ye, B. H. Lee, *Front. Soft Matter* **2023**, *2*, 1101680.
[30] H. Shirahama, B. H. Lee, L. P. Tan, N.-J. Cho, *Sci. Rep.* **2016**, *6*, 31036.
[31] N. Formisano, C. van der Putten, R. Grant, G. Sahin, R. K. Truckenmüller, C. V. C. Bouten, N. A. Kurniawan, S. Giselbrecht, *Adv. Healthcare Mater.* **2021**, *10*, 2100972.
[32] L. C. Bichara, H. E. Lanús, S. A. Brandán, *J. Chem. Chem. Eng.* **2011**, *5*, 936.
[33] N. Khan, A. K. Singh, A. Saneja, *Foods* **2023**, *12*, 1363.
[34] S. Abdollahi Baghban, M. Ebrahimi, S. Bagheri-Khoulenjani, M. Khorasani, *RSC Adv.* **2021**, *11*, 14996.
[35] R. L. Alexa, H. Iovu, J. Ghitman, A. Serafim, C. Stavarache, M. M. Marin, R. Lanchis, *Polymers (Basel)* **2021**, *13*, 727.
[36] D. Zhao, C. Tie, B. Cheng, S. Yang, X. Wang, Z. Sun, M. Yin, H. Zhu, M. Yin, *Polym. Degrad. Stab.* **2020**, *179*, 109297.
[37] K. M. Faridul Hasan, G. Török, T. C. Ali, P. G. Horváth, M. Bak, T. Alpár, *IOP Conf. Ser.: Mater. Sci. Eng.* **2023**, *1266*, 012011.
[38] M. Palomba, A. Longo, G. Carotenuto, *Mater. Proc.* **2021**, *4*, 33.
[39] P. Erkoc, F. Seker, T. Bagci-Onder, S. Kizilel, *Macromol. Biosci.* **2018**, *18*, 1700369.
[40] S. V. Murphy, A. Atala, *Nat. Biotechnol.* **2014**, *32*, 773.
[41] T. A. Arica, M. Guzelgulgen, A. A. Yildiz, M. M. Demir, *Mater. Sci. Eng., C* **2021**, *120*, 111720.
[42] A. Bagheri, M. Asadi-Eydivand, A. A. Rosser, C. M. Fellows, T. C. Brown, *Adv. Eng. Mater.* **2023**, *25*, 2201785.
[43] M. Ayran, Z. Akdag, S. Ulag, O. Gunduz, *Rom J. Mater.* **2023**, *3*, 189.
[44] W. Zhu, J. Long, M. Shi, *Materials* **2023**, *16*, 3282.
[45] B. A. Wagner, G. R. Buettner, *Adv. Redox Res.* **2023**, *9*, 100077.

